

Tuning transport coefficients of monolayer $MoSi_2N_4$ with biaxial strain

Xiao-Shu Guo(郭小姝) and San-Dong Guo(郭三栋)

Citation: Chin. Phys. B, 2021, 30 (**6**): 067102. DOI: 10.1088/1674-1056/abdb22
Journal homepage: http://cpb.iphy.ac.cn; http://iopscience.iop.org/cpb

What follows is a list of articles you may be interested in

Intercalation of van der Waals layered materials: A route towards engineering of electron correlation

Jingjing Niu(牛晶晶), Wenjie Zhang(章文杰), Zhilin Li(李治林), Sixian Yang(杨嗣贤), Dayu Yan(闫大禹), Shulin Chen(陈树林), Zhepeng Zhang(张哲朋), Yanfeng Zhang(张艳锋), Xinguo Ren(任新国), Peng Gao(高鹏), Youguo Shi(石友国), Dapeng Yu(俞大鹏), Xiaosong Wu(吴孝松)
Chin. Phys. B, 2020, 29 (**9**): 097104. DOI: 10.1088/1674-1056/abab85

Vanadium based XVO_3 (X=Na, K, Rb) as promising thermoelectric materials: First-principle DFT calculations

N A Noor, Nosheen Mushahid, Aslam Khan, Nessrin A. Kattan, Asif Mahmood, Shahid M. Ramay
Chin. Phys. B, 2020, 29 (**9**): 097101. DOI: 10.1088/1674-1056/ab99ad

Effects of layer stacking and strain on electronic transport in two-dimensional tin monoxide

Yanfeng Ge(盖彦峰), Yong Liu(刘永)
Chin. Phys. B, 2019, 28 (**7**): 077104. DOI: 10.1088/1674-1056/28/7/077104

Negative differential resistance and quantum oscillations in $FeSb_2$ with embedded antimony

Fangdong Tang(汤方栋), Qianheng Du(杜乾衡), Cedomir Petrovic, Wei Zhang(张威), Mingquan He(何明全), Liyuan Zhang(张立源)
Chin. Phys. B, 2019, 28 (**3**): 037104. DOI: 10.1088/1674-1056/28/3/037104

Influence of electron-phonon interaction on the properties of transport through double quantum dot with ferromagnetic leads

Luo Kan, Wang Fa-Qiang, Liang Rui-Sheng, Ren Zhen-Zhen
Chin. Phys. B, 2014, 23 (**10**): 107103. DOI: 10.1088/1674-1056/23/10/107103

Tuning transport coefficients of monolayer $MoSi_2N_4$ with biaxial strain*

Xiao-Shu Guo(郭小姝)[1,2] and San-Dong Guo(郭三栋)[1,2,†]

[1] School of Electronic Engineering, Xi'an University of Posts and Telecommunications, Xi'an 710121, China
[2] Key Laboratory of Advanced Semiconductor Devices and Materials, Xi'an University of Posts and Telecommunications, Xi'an 710121, China

(Received 23 November 2020; revised manuscript received 29 December 2020; accepted manuscript online 13 January 2021)

Experimentally synthesized $MoSi_2N_4$ (*Science* **369** 670 (2020)) is a piezoelectric semiconductor. Here, we systematically study the large biaxial (isotropic) strain effects (0.90–1.10) on electronic structures and transport coefficients of monolayer $MoSi_2N_4$ by density functional theory (DFT). With a/a_0 from 0.90 to 1.10, the energy band gap firstly increases, and then decreases, which is due to transformation of conduction band minimum (CBM). Calculated results show that the $MoSi_2N_4$ monolayer is mechanically stable in the considered strain range. It is found that the spin-orbital coupling (SOC) effects on Seebeck coefficient depend on the strain. In unstrained $MoSi_2N_4$, the SOC has neglected influence on Seebeck coefficient. However, the SOC can produce important influence on Seebeck coefficient, when the strain is applied, for example, 0.96 strain. The compressive strain can change relative position and numbers of conduction band extrema (CBE), and then the strength of conduction bands convergence can be enhanced, to the benefit of n-type ZT_e. Only about 0.96 strain can effectively improve n-type ZT_e. Our works imply that strain can effectively tune the electronic structures and transport coefficients of monolayer $MoSi_2N_4$, and can motivate farther experimental exploration.

Keywords: $MoSi_2N_4$, electronic transport, 2D materials

PACS: 71.20.–b, 72.15.Jf **DOI:** 10.1088/1674-1056/abdb22

1. Introduction

The successful exfoliation of graphene[1] induces increasing attention on two-dimensional (2D) materials. Many of them have semiconducting behavior, which has various potential applications in electronics, optoelectronics and piezoelectronics.[2–5] Their electronic structures, heat transport and piezoelectric properties have been widely investigated.[6–16] It has been proved that the strain can effectively tune electronic structures, transport and piezoelectric properties of 2D materials,[15–23] which shows great potential for better use in the nanoelectronic, thermoelectric and piezoelectric applications. For example, both compressive and tensile strains can induce the semiconductor-to-metal transition in monolayer MoS_2.[17] In many monolayers of transition metal dichalchogenides (TMD), the power factor can be enhanced by strain due to bands converge.[15,16,18] With increased tensile strain, the lattice thermal conductivity shows monotonous decrease, up-and-down and jump behavior with similar penta-structures.[19] Strain can also improve the piezoelectric strain coefficient by tuning the elastic and piezoelectric stress coefficients.[20–23]

Recently, the layered 2D $MoSi_2N_4$ and WSi_2N_4 have been experimentally achieved by chemical vapor deposition (CVD).[24] The septuple-atomic-layer MA_2Z_4 monolayers with twelve different structures are constructed by intercalating MoS_2-type MZ_2 monolayer into InSe-type A_2Z_2 monolayer.[25] The 66 thermodynamically and dynamically stable MA_2Z_4 structures are predicted by the first principle calculations. They can be commonly semiconductors, half-metal ferromagnetisms or spin-gapless semiconductors (SGSs), Ising superconductors and topological insulators, which depend on the number of valence electrons.[25] We predict intrinsic piezoelectricity in monolayer MA_2Z_4,[26] which means that MA_2Z_4 family may have potential application in piezoelectric field. Structure effect on intrinsic piezoelectricity in monolayer MSi_2N_4 (M = Mo and W) has also been reported by the first principle calculations.[27] By applied strain, the VSi_2P_4 monolayer undergoes ferromagnetic metal (FMM) to SGS to ferromagnetic semiconductor (FMS) to SGS to ferromagnetic half-metal (FMHM) with increasing strain.[28] Some materials of MA_2Z_4 lack inversion symmetry with a strong SOC effect, which are expected to exhibit rich spin-valley physics.[25] The valley-dependent properties of monolayer $MoSi_2N_4$, WSi_2N_4 and $MoSi_2As_4$ have been predicted by the first-principles calculations.[25,29,30] Recently, Janus 2D monolayer in the new septuple-atomic-layer 2D MA_2Z_4 family has been achieved,[31] which shows Rashba spin splitting and out-of-plane piezoelectric polarizations.

In nanoscale devices, the residual strain usually exists in real applications.[32] In our previous work, the small strain ef-

*Project supported by the Natural Science Basis Research Plan in Shaanxi Province of China (Grant No. 2021JM-456).
†Corresponding author. E-mail: sandongyuwang@163.com
© 2021 Chinese Physical Society and IOP Publishing Ltd

fects (0.96 to 1.04) on piezoelectric coefficients of monolayer $MoSi_2N_4$ have been investigated.[26] In this work, the large (0.90 to 1.10) biaxial strain-tuned electronic structures and transport coefficients of monolayer $MoSi_2N_4$ are studied by the first principle calculations. With a/a_0 from 0.90 to 1.10, the energy band gap of monolayer $MoSi_2N_4$ firstly increases, and then decreases. In n-type doping, the Seebeck coefficient S can be effectively enhanced by applying compressive strain, and then the ZT_e can be improved. The tensile strain can induce flat valence bands around the Γ point near the Fermi level, producing large p-type S. Therefore, our works give an experimental proposal to improve transport coefficients of monolayer $MoSi_2N_4$.

The rest of the paper is organized as follows. In Section 2, we give our computational details and methods about transport coefficients. In Sections 3 and 4, we present the main results of monolayer $MoSi_2N_4$ about strain-tuned electronic structures and transport coefficients. Finally, we present our conclusions in Section 5.

2. Computational detail

To avoid interactions between two neighboring images, a vacuum spacing of more than 32 Å along the z direction is added to construct monolayer $MoSi_2N_4$. The elastic stiffness tensor elements C_{ij} are calculated using strain-stress relationship (SSR), which are performed by employing the VASP code[33,35,38] within the framework of DFT.[36,37] A kinetic cutoff energy of 500 eV is adopted, and we use the popular generalized gradient approximation of Perdew, Burke and Ernzerh of (GGA-PBE)[37] as the exchange–correlation potential to calculate elastic and electronic properties. The total energy convergence criterion is set to 10^{-8} eV, and the Hellmann–Feynman forces on each atom are less than 0.0001 eV$\cdot$Å^{-1}. The Brillouin zone (BZ) sampling is obtained using a Monkhorst–Pack mesh of $15\times15\times1$ for elastic constants C_{ij}. The 2D elastic coefficients C_{ij}^{2D} have been renormalized by the the length of unit cell along z direction (L_z): $C_{ij}^{2D} = L_z C_{ij}^{3D}$.

The electronic transport coefficients of $MoSi_2N_4$ monolayer are calculated by solving the Boltzmann transport equations within the constant scattering time approximation (CSTA), which is performed by the BoltzTrap[39] code. To include the SOC, a full-potential linearized augmented-plane-waves method is used to calculate the energy bands of $MoSi_2N_4$ monolayer, as implemented in the WIEN2k package.[40] To attain accurate transport coefficients, a 35 $\times35\times$ 1 k-point meshes is used in the first BZ for the energy band calculation, make harmonic expansion up to $l_{max} = 10$ in each of the atomic spheres, and set $R_{mt}k_{max} = 8$.

3. Electronic structures

The $MoSi_2N_4$ monolayer can be considered as the insertion of the 2H MoS_2-type MoN_2 monolayer into the α-InSe-type Si_2N_2, and the side and top views of the structure of the $MoSi_2N_4$ monolayer are plotted in Fig. 1. The structure breaks the inversion symmetry, but preserves a horizontal mirror corresponding to the plane of the Mo layer. This leads to that $MoSi_2N_4$ monolayer only has in-plane piezoelectric response, and has not out-of-plane piezoelectric polarizations. Using optimized lattice constants,[26] the energy bands of $MoSi_2N_4$ monolayer using GGA and GGA + SOC are shown in Fig. 2, and exhibit both the indirect band gaps with valence band maximum (VBM) at Γ point and CBM at K point. Due to lacking inversion symmetry and containing the heavy element Mo, there exists an SOC induced spin splitting of about 0.13 eV near the Fermi level in the valence bands at K point. This may provide a platform for spin-valley physics,[25,29,30] but the VBM is not at K point, which can be tuned by strain. According to orbital projected band structure, it is found that the states near the Fermi level are dominated by the Mo d orbitals. More specifically, the states around both CBM and VBM are dominated by the Mo d_{z^2} orbital.

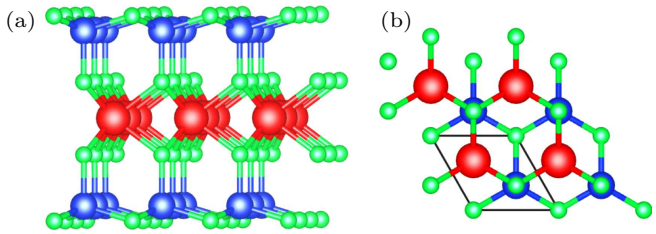


Fig. 1. The crystal structure of monolayer $MoSi_2N_4$ ((a) side view and (b) top view). The primitive cell is are marked by black line, and the large red balls represent Mo atoms, and the middle blue balls for Si atoms, and the small green balls for N atoms.

It is proved that the electronic structures, topological properties, transport and piezoelectric properties of 2D materials can be effectively tuned by strain.[15–23,41] The biaxial strain can be simulated by a/a_0 or $(a-a_0)/a_0$, where a and a_0 are the strained and unstrained lattice constants, respectively. The $a/a_0 < 1$ or $(a-a_0)/a_0 < 0$ means compressive strain, while $a/a_0 > 1$ or $(a-a_0)/a_0 > 0$ implies tensile strain. With a/a_0 from 0.90 to 1.10, the energy band structures are plotted in Fig. 2, and the energy band gap and spin-orbit splitting value Δ at K point are shown in Fig. 3.

It is found that the energy band gap firstly increases (0.90 to 0.96), and then decreases (0.96 to 1.10), which is due to transformation of CBM. Similar phenomena can be observed in many TMD and Janus TMD monolayers.[16,44] With strain

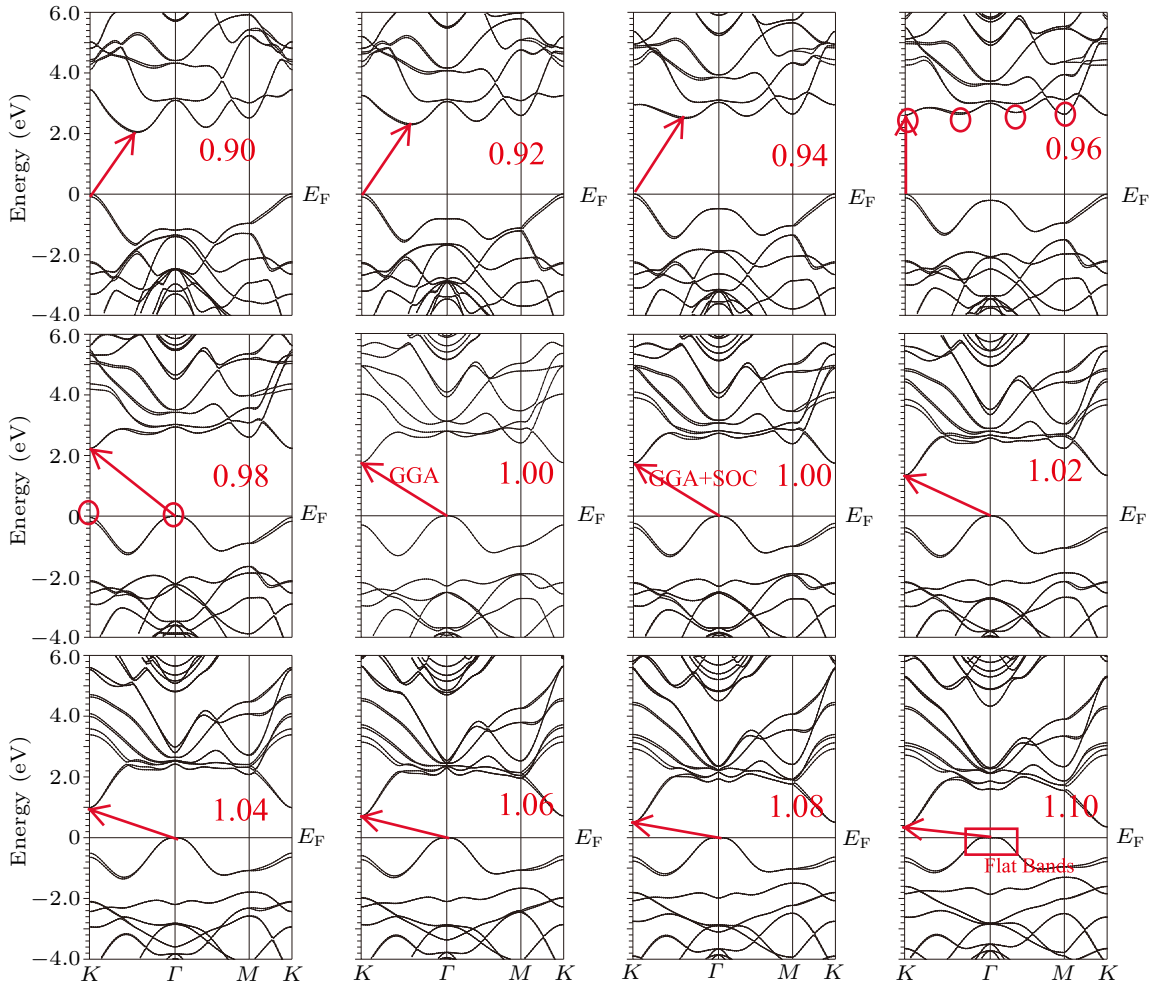


Fig. 2. The energy band structures of monolayer $MoSi_2N_4$ using GGA + SOC with the application of biaxial strain (−10% to 10%), and the unstrained energy band using GGA. The VBM and CBM are marked by arrows. At 0.96 (0.98) strain, four CBE (two VBE) are marked by ellipse.

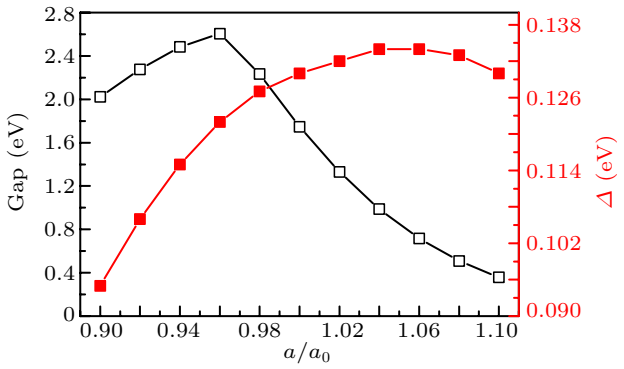


Fig. 3. For $MoSi_2N_4$ monolayer, the energy band gap and spin-orbit splitting value Δ at K point using GGA + SOC as a function of strain.

from compressive one to tensile one, the Δ has a rapid increase, and then a slight decrease. With increasing compressive strain (1.00 to 0.90), the position of CBM (VBM) changes from K (Γ) point to one point along the K–Γ direction (K point), when the compressive strain reaches about 0.94 (0.96). The compressive strain can also tune the numbers and relative positions of valence band extrema (VBE) or CBE. For example, at 0.96, the four CBE can be observed, and their energies are very close, which has very important effects on transport properties. To explore orbital contribution to the conduction bands in the case of 0.96 strain, we project the states to atomic orbitals at 0.96 strained and unstrained conditions, which are shown in Fig. 4. At 0.96 strain, the composition of the low-energy states has little change with respect to unstrained one. At 0.98, the energy of two VBE are nearly the same. The compressive strain can make K point with spin splitting become VBM, which is very useful to allow spin manipulation for spin-valley physics. For example, at 0.94 strain, the VBM at K point is 0.49 eV higher than that at Γ point. It is clearly seen that the increasing tensile strain can make valence band around the Γ point near the Fermi level more flat.

Finally, the elastic constants C_{ij} are calculated as a function of a/a_0 to study the mechanical stability of $MoSi_2N_4$ monolayer with strain. For 2D hexagonal crystals, the Born criteria of mechanical stability[45] ($C_{11} > 0$ and $C_{66} > 0$) should be satisfied. The calculated C_{11} and C_{66} as a function of strain are plotted in Fig. 5, and it is clearly seen that the $MoSi_2N_4$ monolayer in considered strain range is mechanically stable, which is very important for farther experimental exploration.

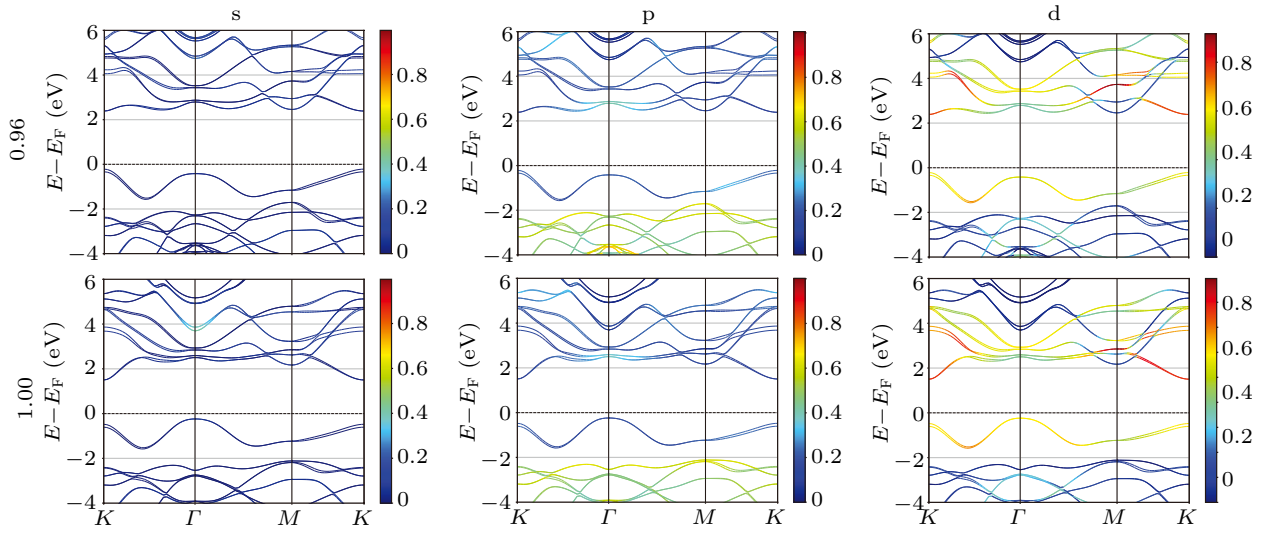


Fig. 4. For $MoSi_2N_4$ monolayer, the orbital projected band structure at 0.96 strained and unstrained conditions.

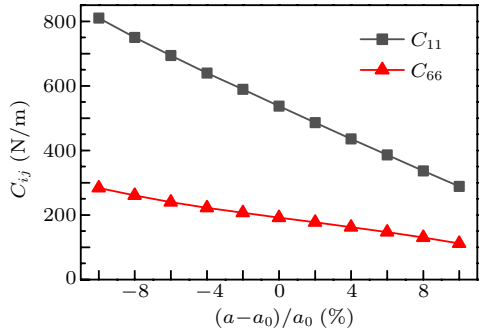


Fig. 5. For $MoSi_2N_4$ monolayer, the elastic constants C_{11} and C_{66} vs. a/a_0 from 0.90 to 1.10.

4. Electronic transport property

Proposed by Hicks and Dresselhaus in 1993,[42,43] the potential thermoelectric materials can be achieved in the low-dimensional systems or nanostructures. The dimensionless figure of merit, $ZT = S^2\sigma T/(\kappa_e + \kappa_L)$, can be used to measure the efficiency of thermoelectric conversion of a thermoelectric material, where S, σ, T, κ_e, and κ_L are the Seebeck coefficient, electrical conductivity, working temperature, electronic and lattice thermal conductivities, respectively. It is noted that, for the 2D material, the calculated σ, κ_e and κ_L depend on L_z (here, $L_z = 40$ Å), and the S and ZT is independent of L_z. For 2D materials, we use electrons or holes per unit cell instead of doping concentration, which is described by N, and the $N < 0$ ($N > 0$) mean n-type (p-type) doping. It is proved that the SOC has important effects on transport coefficients of TMD and Janus TMD monolayers.[16,18,44] However, the SOC has neglectful influences on transport properties of unstrained $MoSi_2N_4$ monolayer, which can be observed from typical Seebeck coefficient S in Fig. 6.

This is because the energy bands near the Fermi level between GGA and GGA + SOC are nearly the same. However, the SOC has an important effect on p-type transport coefficients under the condition of compressive strain. For example, at 0.96 strain, a detrimental effect on Seebeck coefficient S can be observed, when including SOC (see Fig. 6). This is because the SOC can remove the band degeneracy near the VBM. Thus, the SOC is included to investigate the biaxial strain effects on transport coefficients of $MoSi_2N_4$ monolayer.

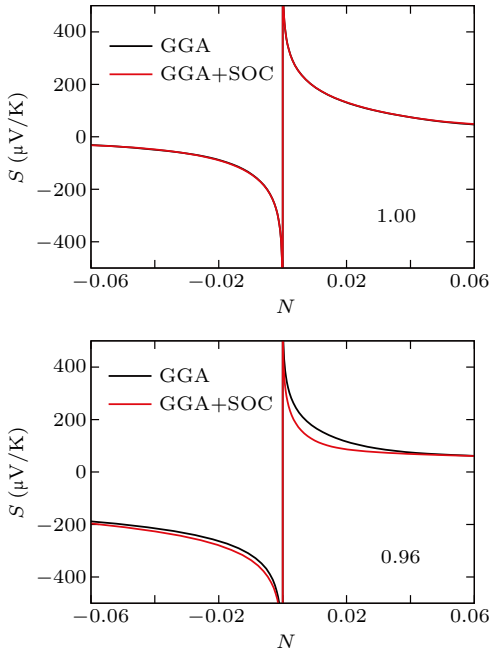


Fig. 6. For $MoSi_2N_4$ monolayer, the room-temperature Seebeck coefficient S using GGA and GGA + SOC at 1.00 and 0.96 strains as a function of doping level N with N being the number of electrons or holes per unit cell.

Using GGA + SOC, the room temperature S, σ/τ and $S^2\sigma/\tau$ of $MoSi_2N_4$ monolayer under different strains (0.90 to 1.10) are shown in Fig. 7. It is clearly seen that the compressive strain has important effects on S, especially for n-type doping. However, the tensile strain produces small influences on S, especially for n-type S. These can be explained by strain-induced energy bands. When the strain is less than or equal to about 0.98, the n-type S (absolute value) can be observably

improved, which is due to compressive strain-driven accidental conduction band degeneracies, namely bands convergence. With expanding compressive strain, in the low doping, the p-type S firstly increases, and has almost no change. This is because the valence bands convergence can be observed at about 0.98, and then is removed (at 0.98, the energies of two VBE are nearly the same, and only one VBE near the Fermi level can be observed with compressive strain from 0.96 to 0.90). For the considered tensile strain, the conduction bands near the Fermi level have little change, which leads to almost unchanged n-type S. When the strain changes from 1.00 to 1.10, the p-type S increases, which is due to tensile strain-induced more flat valence bands around Γ point near the Fermi level. This can be understood by $S = \frac{8\pi^2 K_B^2}{3eh^2} m^* T (\frac{\pi}{3n})^{2/3}$, in which m^*, T and n are the effective mass of the carrier, temperature and carrier concentration, respectively. The flat bands can produce very large effective mass of the carrier, which will lead to improved S. It is found that the strain has nearly the opposite effects on σ/τ with respect to S. It is found that the compressive strain can dramatically improve $S^2\sigma/\tau$ due to the strain-enhanced S.

An upper limit of ZT can be measured by $ZT_e = S^2\sigma T/\kappa_e$, neglecting the κ_L. The room-temperature ZT_e of $MoSi_2N_4$ monolayer under different strains as a function of doping level is also shown in Fig. 7. The calculated results show that the dependence of ZT_e is very similar to S (absolute value), which can be explained by the Wiedemann–Franz law: $\kappa_e = L\sigma T$ (L is the Lorenz number). Then the ZT_e can be reformulated by $ZT_e = S^2/L$. Thus, the strain-induced bands convergence improves S, which is beneficial to better ZT_e.

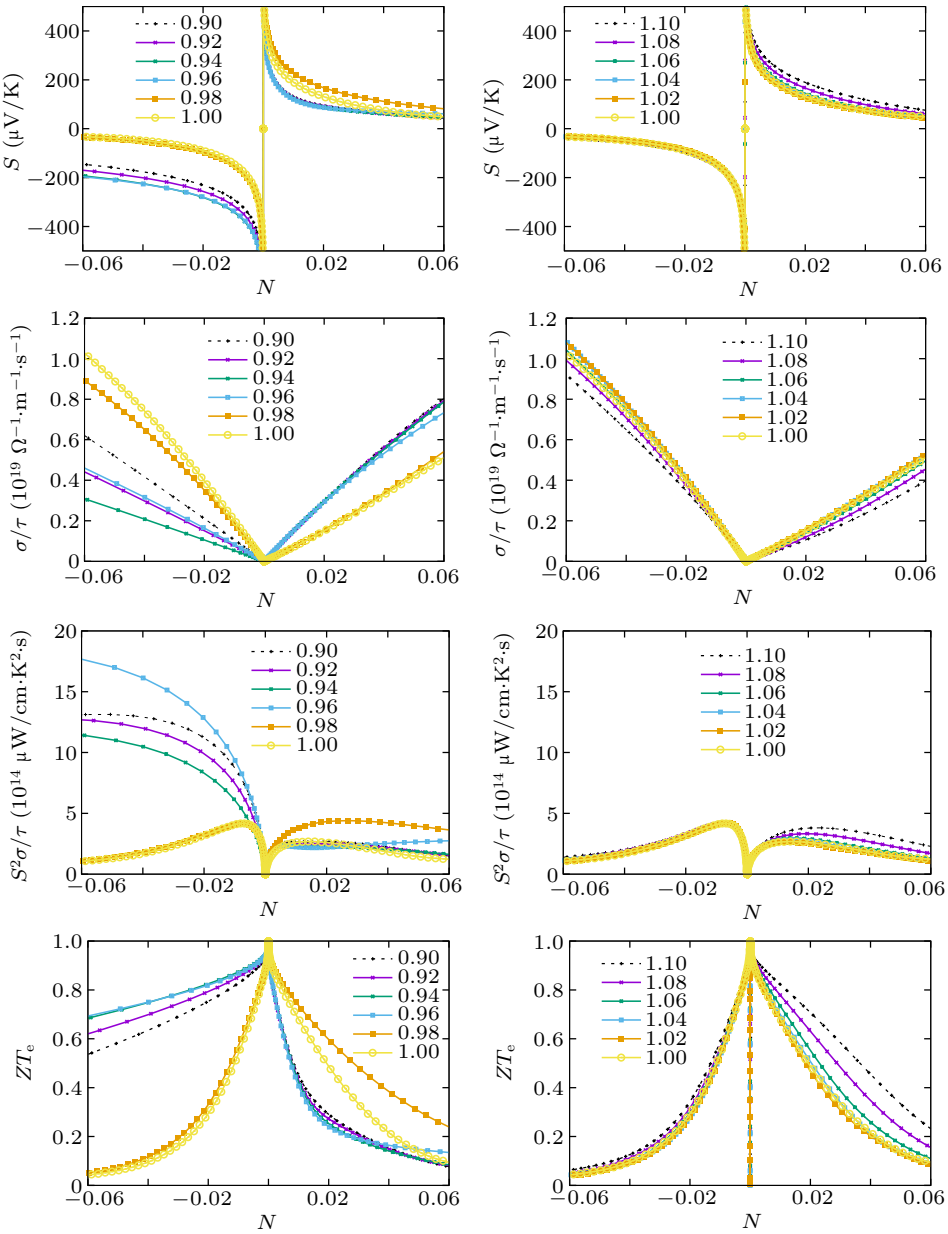


Fig. 7. For $MoSi_2N_4$ monolayer, the room-temperature transport coefficients with the a/a_0 from 0.90 to 1.10, i.e., Seebeck coefficient S, electrical conductivity with respect to scattering time σ/τ, power factor with respect to scattering time $S^2\sigma/\tau$ and ZT_e (an upper limit of ZT) as a function of doping level N using GGA + SOC. Left: compressive strain. Right: tensile strain.

5. Conclusion

In summary, we have investigated the biaxial strain (0.90 to 1.10) effects on electronic structures and transport coefficients of monolayer $MoSi_2N_4$ by the reliable first-principles calculations. With the strain from 0.90 to 1.10, the energy band gap of $MoSi_2N_4$ monolayer shows a nonmonotonic behavior. It is found that the SOC has little effects on transport coefficients of unstrained $MoSi_2N_4$ in the considered doping range due to the hardly changed dispersion of bands near the Fermi level. However, the SOC has very important influences on transport properties of strained $MoSi_2N_4$, for example, 0.96 strain, which is due to the position change of VBM. The calculated results show that compressive strain can tune the numbers and relative positions of CBE, which can lead to enhanced n-type S, and then better n-type ZT_e. Our work may provide an idea to optimize the electronic structures and transport properties of monolayer $MoSi_2N_4$.

Acknowledgments

We are grateful to the Advanced Analysis and Computation Center of China University of Mining and Technology (CUMT) for the award of CPU hours and WIEN2k/VASP software to accomplish this work.

References

[1] Novoselov K S, Geim A K, Morozov S V *et al*. 2004 *Science* **306** 666
[2] Mak K F and Shan J 2016 *Nat. Photon.* **10** 216
[3] Blonsky M N, Zhuang H L, Singh A K and Hennig R G 2015 *ACS Nano* **9** 9885
[4] Hui Z Q, Xu W X, Li X H *et al*. 2019 *Nanoscale* **11** 6045
[5] Wu W and Wang Z L 2016 *Nat. Rev. Mater.* **1** 16031
[6] Chhowalla M, Shin H S, Eda G, Li L J, Loh K P and Zhang H 2013 *Nat. Chem.* **5** 263
[7] Lu A Y, Zhu H Y, Xiao J *et al*. 2017 *Nat. Nanotechnol.* **12** 744
[8] Fei R X, Li W B, Li J and Yang L 2015 *Appl. Phys. Lett.* **107** 173104
[9] Zhang S L *et al*. 2016 *Angew. Chem.* **128** 1698
[10] Blonsky M N, Zhuang H L, Singh A K and Hennig R G 2015 *ACS Nano* **9** 9885
[11] Fei R X, Li W B, Li J and Yang L 2015 *Appl. Phys. Lett.* **107** 173104
[12] Duerloo K N, Ong M T and Reed E J 2012 *J. Phys. Chem. Lett.* **3** 2871
[13] Chen Y, Liu J Y, Yu J B, Guo Y G and Sun Q 2019 *Phys. Chem. Chem. Phys.* **21** 1207
[14] Ji J P *et al*. 2016 *Nat. Commun.* **7** 13352
[15] Lv H Y, Lu W J, Shao D F, Lub H Y and Sun Y P 2016 *J. Mater. Chem. C* **4** 4538
[16] Guo S D 2016 *J. Mater. Chem. C* **4** 9366
[17] Scalise E, Houssa M, Pourtois G, Afanas'ev V and Stesmans A 2012 *Nano Res.* **5** 43
[18] Guo S D 2016 *Comput. Mater. Sci.* **123** 8
[19] Liu H K, Qin G Z, Lin Y and Hu M 2016 *Nano Lett.* **16** 3831
[20] Jena N, Dimple, Behere S D and Sarkar A D 2017 *J. Phys. Chem. C* **121** 9181
[21] Guo S D, Guo X S, Zhang Y Y and Luo K 2020 *J. Alloys Compd.* **822** 153577
[22] Dimple, Jena N, Rawat A, Ahammed R, Mohanta M K and Sarkar A D 2018 *J. Mater. Chem. A* **6** 24885
[23] Guo S D, Mu W Q and Zhu Y T 2021 *J. Phys. Chem. Solids* **151** 109896
[24] Hong Y L, Liu Z B, Wang L *et al*. 2020 *Science* **369** 670
[25] Wang L, Shi Y P, Liu M F *et al*. 2020 arXiv:2008.02981
[26] Guo S D, Zhu Y T, Mu W Q and Ren W C 2021 *Europhys. Lett.* **132** 57002
[27] Guo S D, Zhu Y T, Mu W Q, Wang L and Chen X Q 2021 *Comput. Mater. Sci.* **188** 110223
[28] Guo S D, Mu W Q, Zhu Y T and Chen X Q 2020 *Phys. Chem. Chem. Phys.* **22** 28359
[29] Li S, Wu W K, Feng X L *et al*. 2020 arXiv:2009.13253
[30] Yang C, Song Z G, Sun X T and Lu J 2020 arXiv:2010.10764
[31] Guo S D, Mu W Q, Zhu Y T, Han R Y and Ren W C 2021 *J. Mater. Chem. C* **9** 2464
[32] Bhowmick S and Shenoy V B 2006 *J. Chem. Phys.* **125** 164513
[33] Kresse G 1995 *J. Non-Cryst. Solids* **193** 222
[34] Kresse G and Furthmüller J 1996 *Comput. Mater. Sci.* **6** 15
[35] Kresse G and Joubert D 1999 *Phys. Rev. B* **59** 1758
[36] Hohenberg P and Kohn W 1964 *Phys. Rev.* **136** B864
[37] Kohn W and Sham L J 1965 *Phys. Rev.* **140** A1133
[38] Perdew J P, Burke K and Ernzerhof M 1996 *Phys. Rev. Lett.* **77** 3865
[39] Madsen G K H and Singh D J 2006 *Comput. Phys. Commun.* **175** 67
[40] Blaha P, Schwarz K, Madsen G K H, Kvasnicka D and Luitz J 2001 *WIEN2k, an Augmented Plane Wave + Local Orbitals Program for Calculating Crystal Properties* (Karlheinz Schwarz Technische Universityät Wien, Austria)
[41] Zhang S L, Xie M Q, Cai B *et al*. 2016 *Phys. Rev. B* **93** 245303
[42] Hicks L D and Dresselhaus M S 1993 *Phys. Rev. B* **47** 12727
[43] Hicks L D and Dresselhaus M S 1993 *Phys. Rev. B* **47** 16631
[44] Guo S D and Dong J 2018 *Semicond. Sci. Technol.* **33** 085003
[45] Andrew R C, Mapasha R E, Ukpong A M and Chetty N 2012 *Phys. Rev. B* **85** 125428